coatings

MDPI

Article

High-Temperature Corrosion of AlCrSiN Film in Ar-1%SO_2 Gas

Poonam Yadav [1], Dong Bok Lee [1,*], Yue Lin [2], Shihong Zhang [2] and Sik Chol Kwon [3]

1 School of Advanced Materials Science & Engineering, Sungkyunkwan University, Suwon 16419, Korea; poonamtusha@gmail.com
2 School of Materials Science & Engineering, Anhui University of Technology, Maanshan 243002, China; tougaoyouxiang206@163.com (Y.L.); shzhang@ahut.edu.cn (S.Z.)
3 Department of Advanced Materials Engineering, Chungbuk National University, Cheongju 28644, Korea; kwonsikchol@chungbuk.ac.kr
* Correspondence: dlee@skku.ac.kr; Tel.: +82-31-290-7355

Academic Editors: Niteen Jadhav and Andrew J. Vreugdenhil
Received: 26 December 2016; Accepted: 9 March 2017; Published: 13 March 2017

Abstract: AlCrSiN film with a composition of 29.1Al-17.1Cr-2.1Si-51.7N in at. % was deposited on a steel substrate by cathodic arc ion plating at a thickness of 1.8 μm. It consisted of nanocrystalline *hcp*-AlN and *fcc*-CrN, where a small amount of Si was dissolved. Corrosion tests were carried out at 800 °C for 5–200 h in Ar-1%SO_2 gas. The major corrosion reaction was oxidation owing to the high oxygen affinity of Al and Cr in the film. The formed oxide scale consisted primarily of $(Al,Cr)_2O_3$, within which Fe, Si, and S were dissolved. Even after corrosion for 200 h, the thickness of the scale was about 0.7–1.2 μm, indicating that the film had good corrosion resistance in the SO_2-containing atmosphere.

Keywords: AlCrSiN film; oxidation; sulfidation; SO_2 gas corrosion

1. Introduction

Aluminum nitride films have good oxidation resistance due to the formation of Al_2O_3 scale [1]. Their properties can be enhanced by alloying with the transition metal Cr. AlCrN films have been applied on dies, molds, and cutting tools [2] for their high hardness [3], thermal stability [4], good resistance to wear [5], and oxidation [6–9]. AlCrN films were oxidized to Al_2O_3 and Cr_2O_3 [6], or $(Cr,Al)_2O_3$ [9], which suppressed oxygen diffusion. The addition of Si to the AlCrN films refines the grain [10,11], decreases crystallinity [11], increases hardness [12,13], and improves the resistance to wear [10] and oxidation [13–15]. AlCrSiN films have been deposited on cemented carbides [11,13,16], Si [11,12,15], and steel [10–12,17] by cathodic arc evaporation [11,16,17], cathodic arc ion plating [10], and magnetron sputtering [13,15]. The high-temperature oxidation of AlCrSiN films in air results in the formation of thin, dense oxide layers consisting primarily of Cr_2O_3 [17], (Cr_2O_3, Al_2O_3) [14], and (Cr_2O_3, Cr_2O_5, Al_2O_3) [13]. However, the corrosion behavior of AlCrSiN films in various corrosive environments needs be investigated for broad applications. In this study, the high-temperature corrosion of AlCrSiN film in a SO_2-containing atmosphere was performed, with an emphasis on TEM/EDS analyses. Resistance to sulfur-containing atmospheres is vital for utilizing AlCrSiN as the protective coating in petrochemical plants, coal-gasification units, turbines, and heat exchangers. Sulfur in SO_2 can induce serious corrosion by forming non-protective, highly non-stoichiometric sulfide scales [18]. In this study, corrosion tests were carried out on AlCrSiN film at 800 °C for 5–200 h in Ar-1%SO_2 gas. The microstructure, corrosion products, and corrosion mechanism of the AlCrSiN film are discussed.

2. Experimental Section

AlCrSiN film was deposited on a steel substrate (AISI M2 high speed steel; Fe-6W-5Mo-4Cr-2V in wt %) by cathodic arc ion plating using Cr and $Al_{88}Si_{12}$ cathodes. It was deposited for 5 h at a nitrogen pressure of 1 Pa, a temperature of 400 °C, a bias voltage of −150 V, an arc current of 55 A, and a cathode-to-substrate distance of 7 cm. The rotation speed of the sample holder was 3 rpm, and an AlCrN interlayer was deposited between the film and the substrate for 20 min. The coated samples were corroded at 800 °C for 5–200 h in the flowing Ar-1%SO_2 gas inside the quartz reaction tube, which was heated inside a tube furnace. Following corrosion, the coated samples were inspected using a scanning electron microscope (SEM), Auger electron spectrometer (AES), X-ray photoelectron spectrometer (XPS), and transmission electron microscope (TEM operated at 200 keV) equipped with an energy dispersive spectrometer (EDS with 5 nm spot size). The TEM samples were prepared by milling using a focused ion beam system after carbon coating.

3. Results and Discussion

Figure 1 shows the TEM/SAED/EDS results of the as-deposited AlCrSiN film, the composition of which was 29.1Al-17.1Cr-2.1Si-51.7N in at. % according to the electron probe microanalysis (EPMA). The AlCrSiN film was 1.8 μm thick, single-layered (Figure 1a), and consisted of nanocrystalline *hcp*-AlN and *fcc*-CrN (Figure 1b). It is known that the crystal structure of CrAlN films changes from B1-*fcc* to B4-*hcp* above the AlN concentration of 65–75 at. % [6], and the addition of Si to CrAlN films facilitates the formation of *hcp*-AlN [16]. In this study, the nucleation of *hcp*-AlN seemed to be accelerated by Si. In Figure 1c, the AlN-rich area was brighter than the CrN-rich area because Al has a lower scattering factor than Cr. Si dissolved rather uniformly in the film, as shown in Figure 1d. Here, the presence of nitrogen in the film was ignored, because TEM/EDS could not accurately quantify the light element.

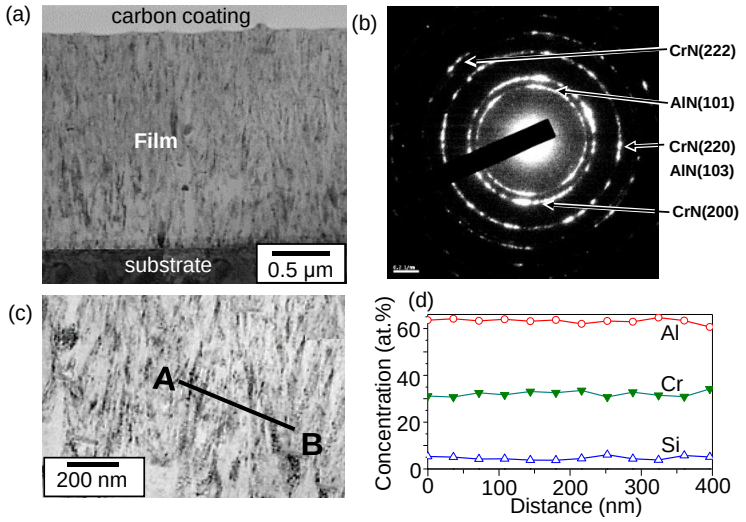

Figure 1. As-deposited AlCrSiN film. (**a**) TEM cross-sectional image; (**b**) selected area electron diffraction (SAED) pattern of the film; (**c**) enlarged TEM image of the film; (**d**) EDS concentration profiles along A-B shown in (c).

Gold was deposited on the AlCrSiN film using a sputter, and corroded at 800 °C for 5 h in order to understand the corrosion mechanism of the AlCrSiN film at the early corrosion stage. In Figure 2, the highest point of Au indicates the original film surface. During corrosion, nitrogen diffused outwardly from the film, while oxygen and sulfur diffused inwardly. Oxygen diffused dominantly and deeply, while sulfur was present only at the outermost surface. The ingress of sulfur through compact oxides could be limited, because the solubility of sulfur in most oxides is very limited [19]. It is worth noting that oxides are thermodynamically more stable than the corresponding sulfides. Since Al is more active

than Cr, Al oxidized predominantly underneath the Au film. Silicon was weakly and non-uniformly present in the film.

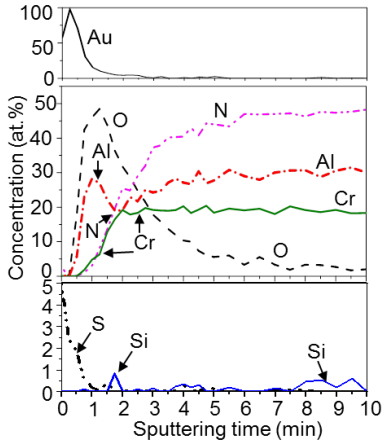

Figure 2. AES depth profiles of the AlCrSiN film after corrosion at 800 °C for 5 h in Ar-1%SO_2 gas. The penetration rate is 19 nm/min for the reference SiO_2.

Figure 3 shows the TEM/EDS results of the AlCrSiN film after corrosion at 800 °C for 10 h. The scale was 0.2 µm thick, reflecting the good corrosion resistance of the AlCrSiN film (Figure 3a). Oxide whiskers protruded over angular oxide grains (Figure 3b). According to the TEM/EDS spot analysis, the scale consisted of $(Al,Cr)_2O_3$ grains with dissolved Fe and Si ions (Figure 3c). Chromia and α-Al_2O_3 are miscible because they have the same corundum structure. The amount of Si shown in Figure 3c is inaccurate, because the spurious Si signal can come out from the EDS detector owing to the internal fluorescence. Iron diffused outward from the substrate through the nanocrystalline film toward the surface according to the concentration gradient. Since oxidation occurred preferentially owing to the thermodynamic stability of the oxides, sulfur was absent in Figure 3c. The XPS analysis, however, identified 2.6 at. %S at the surface of the $(Al,Cr)_2O_3$ scale. Such a discrepancy in the chemical composition of the oxide scale at the surface was attributed to the different detectability of XPS and TEM-EDS.

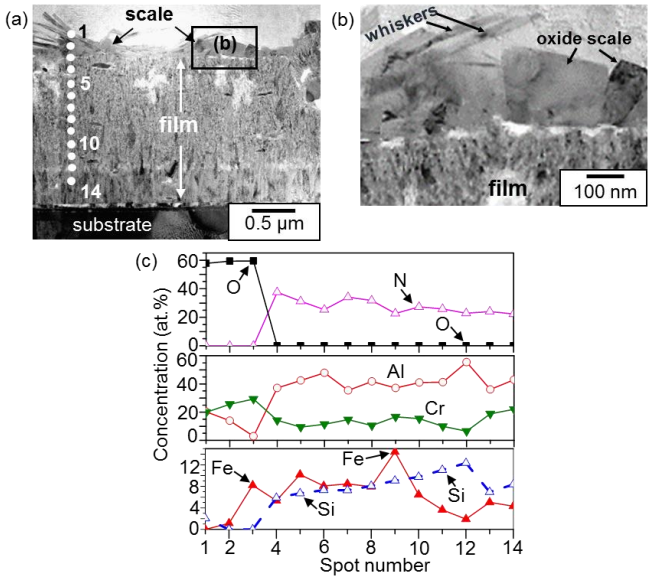

Figure 3. AlCrSiN film after corrosion at 800 °C for 10 h in Ar-1%SO_2 gas. (**a**) TEM cross-sectional image, (**b**) enlarged image of rectangular area shown in (a), (**c**) EDS concentration profiles along the spots 1–14.

Figure 4 shows the TEM/EDS results of the AlCrSiN film after corrosion at 800 °C for 50 h. The scale was still thin because of the formation of the slowly growing oxide scale (Figure 4a). Spots 1–3 and 4–9 corresponded to the (Fe, Si, S)-dissolved $(Al,Cr)_2O_3$ scale and the S-free, (Fe, O)-dissolved AlCrSiN film, respectively (Figure 4b). Nitrogen was absent around the oxide scale. The concentrations shown in Figure 4b are, however, suspicious, because of the difficulty in quantifying nitrogen, oxygen, and Si. Nonetheless, sulfur was detected at the outer part of the scale. The inward diffusion of oxygen through the nanocrystalline film led to the dissolution of rather a large amount of oxygen in the film. The oxide grains shown in Figure 4a were tens of nanometers in diameter. Dissolution of foreign ions such as Fe and Si can facilitate the rapid establishment of the protective $(Al,Cr)_2O_3$ scale by increasing the defect concentration through the doping effect. The protruded oxides at spots 1 and 2 were evidently formed by the outward diffusion of Cr, Al, Fe, and Si. Hence, it is seen that the corrosion proceeded not only by the inward transport of oxygen (see Figure 2) but also by the outward diffusion of cations from the film and the substrate (see Figures 3 and 4). At the outer part of the scale, Cr was frequently richer than Al, suggesting that Cr tended to diffuse outwardly faster than Al.

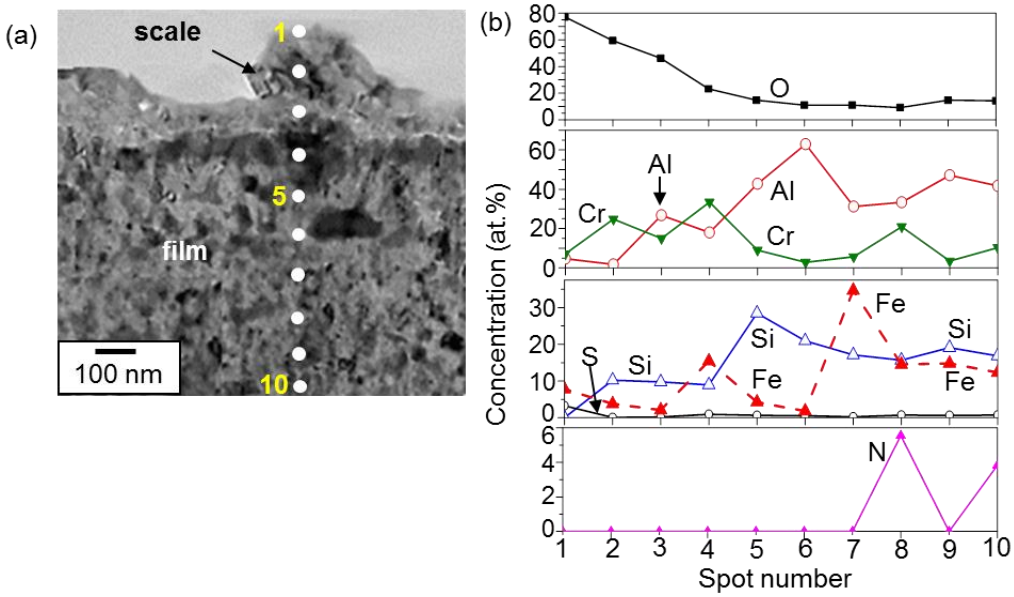

Figure 4. AlCrSiN film after corrosion at 800 °C for 50 h. (**a**) TEM cross-sectional image; (**b**) EDS concentration profiles along the spots 1–10.

The SEM/TEM/EDS results of the AlCrSiN film at the later stage of corrosion are shown in Figure 5. The surface of the scale was covered with angled, round, and rod-shaped oxide grains (Figure 5a). Spots 1–4 shown in Figure 5b show a rod-shaped $(Al,Cr)_2O_3$ grain dissolved with Fe, Si, and S (Figure 5c). Al, Cr, Fe, and Si clearly diffused outwards to spots 1–4. The ratio of Al/Cr in the oxide scale fluctuated depending on the location, as shown in Figure 5c. For example, spots 1–4 are Al-rich, while spots 5 and 6 are Cr-rich. More frequently, Cr-rich oxide scale formed on the Al-rich oxide scale. Spot 7 indicates that the $(Al,Cr)_2O_3$ oxide contained some Si, S, and N. At spot 8, the nitride film began to oxidize. Spots 9–14 corresponded to the (Fe, O, S)-dissolved AlCrSiN film.

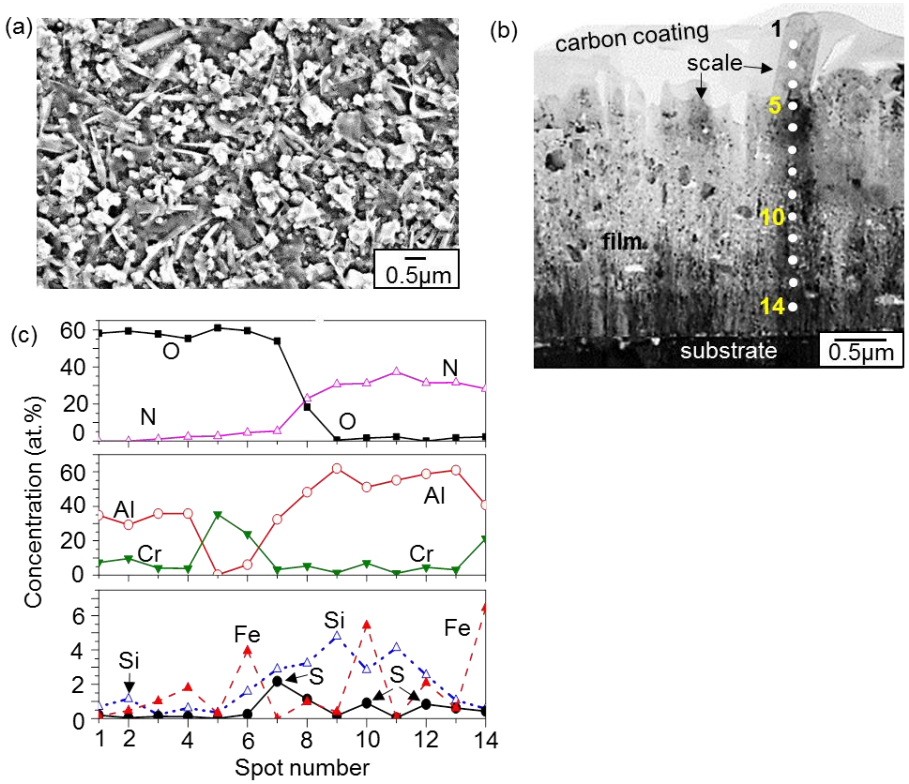

Figure 5. AlCrSiN film after corrosion at 800 °C for 200 h in Ar-1%SO_2 gas. (**a**) SEM top view; (**b**) TEM cross-sectional image; (**c**) EDS concentration profiles along the spots 1–14.

4. Conclusions

The AlCrSiN film was single-layered, and consisted of nanocrystalline *hcp*-AlN and *fcc*-CrN, which had a small amount of dissolved Si. Its corrosion behavior was studied at 800 °C for 5–200 h in Ar-1% SO_2 gas. At the early corrosion stage, Al oxidized preferentially at the surface. As the corrosion proceeded, the competitive oxidation of Al and Cr led to the formation of $(Al,Cr)_2O_3$ grains with or without dissolved ions of Fe, Si, and S. The $(Al,Cr)_2O_3$ scale effectively protected the film. The corrosion proceeded not only by the inward transport of oxygen and sulfur, but also by the outward diffusion of Al, Cr, Si, and N from the film as well as Fe from the substrate. Compared to sulfur, oxygen diffused dominantly and deeply into the film. The surface of the scale was covered with angled, round, and rod-shaped oxide grains.

Acknowledgments: This work was supported under the framework of the international cooperation program managed by the National Research Foundation of Korea (2016K2A9A1A01952060).

Author Contributions: Yue Lin, Shihong Zhang and Sik Chol Kwon synthesized the coatings by cathodic arc ion plating. Poonam Yadav did the corrosion test and analyzed the results. Dong Bok Lee supervised the work.

Conflicts of Interest: The authors declare no conflict of interest.

References

1. Lin, C.Y.; Lu, F.H. Oxidation behavior of AlN films at high temperature under controlled atmosphere. *J. Eur. Ceram. Soc.* **2008**, *28*, 691–698. [CrossRef]
2. Fox-Rabinovich, G.S.; Beake, B.D.; Endrino, J.L.; Veldhuis, S.C.; Parkinson, R.; Shuster, L.S.; Migranov, M.S. Effect of mechanical properties measured at room and elevated temperatures on the wear resistance of cutting tools with TiAlN and AlCrN coatings. *Surf. Coat. Technol.* **2006**, *200*, 5738–5742. [CrossRef]
3. Bourhis, E.L.; Goudeau, P.; Staia, M.H.; Carrasquero, E.; Puchi-Cabrera, E.S. Mechanical properties of hard AlCrN-based coated substrates. *Surf. Coat. Technol.* **2009**, *203*, 2961–2968. [CrossRef]

4. Willmann, H.; Mayrhofer, P.H.; Persson, P.O.A.; Reiter, A.E.; Hultman, L.; Mitterer, C. Thermal stability of Al–Cr–N hard coatings. *Scr. Mater.* **2006**, *54*, 1847–1851. [CrossRef]
5. Ding, X.Z.; Zeng, X.T. Structural, mechanical and tribological properties of CrAlN coatings deposited by reactive unbalanced magnetron sputtering. *Surf. Coat. Technol.* **2005**, *200*, 1372–1376. [CrossRef]
6. Reiter, A.E.; Derflinger, V.H.; Hanselmann, B.; Bachmann, T.; Sartory, B. Investigation of the properties of $Al_{1-x}Cr_xN$ coatings prepared by cathodic arc evaporation. *Surf. Coat. Technol.* **2005**, *200*, 2114–2122. [CrossRef]
7. Kawate, M.; Hashimoto, A.K.; Suzuki, T. Oxidation resistance of CrAlN and TiAlN films. *Surf. Coat. Technol.* **2003**, *165*, 163–167. [CrossRef]
8. Hirai, M.; Ueno, Y.; Suzuki, T.; Jiang, W.; Grigoriu, C.; Yatsui, K. Characteristics of (Cr_{1-x}, Al_x)N films prepared by pulsed laser deposition. *Jpn. J. Appl. Phys.* **2001**, *40*, 1056–1060. [CrossRef]
9. Banakh, O.; Schmid, P.E.; Sanjinés, R.; Lévy, F. High-temperature oxidation resistance of $Cr_{1-x}Al_xN$ thin films deposited by reactive magnetron sputtering. *Surf. Coat. Technol.* **2003**, *163*, 57–61. [CrossRef]
10. Wu, W.; Chen, W.; Yang, S.; Lin, Y.; Zhang, S.; Cho, T.Y.; Lee, G.H.; Kwon, S.C. Design of AlCrSiN multilayer and nanocomposite coating for HSS cutting tools. *Appl. Surf. Sci.* **2015**, *351*, 803–810. [CrossRef]
11. Soldán, J.; Neidhardt, J.; Sartory, B.; Kaindl, R.; Čerstvý, R.; Mayrhofer, P.H.; Tessadri, R.; Polcik, P.; Lechthaler, M.; Mitterer, C. Structure–property relations of arc-evaporated Al–Cr–Si–N coatings. *Surf. Coat. Technol.* **2008**, *202*, 3555–3562. [CrossRef]
12. Tritremmel, C.; Daniel, R.; Lechthaler, M.; Polcik, P.; Mitterer, C. Influence of Al and Si content on structure and mechanical properties of arc evaporated Al–Cr–Si–N thin films. *Thin Solid Films* **2013**, *534*, 403–409. [CrossRef]
13. Bobzin, K.; Bagcivan, N.; Immich, P.; Bolz, S.; Cremer, R.; Leyendecker, T. Mechanical properties and oxidation behaviour of (Al, Cr)N and (Al, Cr, Si)N coatings for cutting tools deposited by HPPMS. *Thin Solid Films* **2008**, *517*, 1251–1256. [CrossRef]
14. Endrino, J.L.; Fox-Rabinovich, G.S.; Reiter, A.; Veldhuis, S.V.; Galindo, R.E.; Albella, J.M.; Marco, J.F. Oxidation tuning in AlCrN coatings. *Surf. Coat. Technol.* **2005**, *201*, 4505–4511. [CrossRef]
15. Chen, H.W.; Chan, Y.C.; Lee, J.W.; Duh, J.G. Oxidation behavior of Si-doped nanocomposite CrAlSiN coatings. *Surf. Coat. Technol.* **2010**, *205*, 1189–1194. [CrossRef]
16. Endrino, J.L.; Palacín, S.; Aguirre, M.H.; Gutiérrez, A.; Schäfers, F. Determination of the local environment of silicon and the microstructure of quaternary CrAl(Si)N films. *Acta Mater.* **2007**, *55*, 2129–2135. [CrossRef]
17. Polcar, T.; Cavaleiro, A. High temperature properties of CrAlN, CrAlSiN and AlCrSiN coatings—Structure and oxidation. *Mater. Chem. Phys.* **2011**, *129*, 195–201. [CrossRef]
18. Birks, N.; Meier, G.H.; Pettit, F.S. *Introduction to the High-Temperature Oxidation of Metals*, 2nd ed.; Cambridge University Press: Cambridge, UK, 2006.
19. Grabke, H.J. High temperature corrosion in complex, multi-reactant gaseous environments. In *High Temperature Materials Corrosion in Coal Gasification Atmospheres*; Norton, J.F., Ed.; Elsevier Applied Science Publishers: London, UK, 1984; pp. 59–82.